NUMERICAL INVESTIGATION OF NUCLEATE POOL BOILING HEAT TRANSFER

by

Andrijana D. STOJANOVIĆ[a]*, Vladimir D. STEVANOVIĆ[b], Milan M. PETROVIĆ[b], and Dragoljub S. ŽIVKOVIĆ[c]

[a] Laboratory for Thermal Energy and Engineering, Vinca Institute of Nuclear Sciences, University of Belgrade, Serbia
[b] Faculty of Mechanical Engineering, University of Belgrade, Belgrade, Serbia
[c] Faculty of Mechanical Engineering, University of Nis, Nis, Serbia

Original scientific paper
DOI: 10.2298/TSCI160404276S

Multi-dimensional numerical simulation of the atmospheric saturated pool boiling is performed. The applied modelling and numerical methods enable a full representation of the liquid and vapour two-phase mixture behaviour on the heated surface, with included prediction of the swell level and heated wall temperature field. In this way the integral behaviour of nucleate pool boiling is simulated. The micro conditions of bubble generation at the heated wall surface are modelled by the bubble nucleation site density, the liquid wetting contact angle and the bubble grow time. The bubble nucleation sites are randomly located within zones of equal size, where the number of zones equals the nucleation site density. The conjugate heat transfer from the heated wall to the liquid is taken into account in wetted heated wall areas around bubble nucleation sites. The boiling curve relation between the heat flux and the heated wall surface temperature in excess of the saturation temperature is predicted for the pool boiling conditions reported in the literature and a good agreement is achieved with experimentally measured data. The influence of the nucleation site density on the boiling curve characteristic is confirmed. In addition, the influence of the heat flux intensity on the spatial effects of vapour generation and two-phase flow are shown, such as the increase of the swell level position and the reduced wetting of the heated wall surface by the heat flux increase.

Key words: *pool boiling, heat flux, modelling*

Introduction

Boiling heat transfer has been a topic of intensive research for decades because of its high efficiency of cooling heated surfaces. Several studies [1-3] focussed on the understanding of the fluid-solid combinations in order to obtain the highest heat fluxes at the minimum wall superheat over the saturation temperature of the boiling liquid. High values of the wall superheat could lead to possible alteration of heat transfer characteristics of the solid wall. However, despite the fact that research has been carried on for several decades, the complete picture of the processes involved is far from complete, due in part to the non-uniformity of the conditions and characteristics of the materials during experiments (heated walls and liquids as well as measuring instrumentation), to the non-linearity of the processes and to the possible

* Corresponding author; e-mail: andrijana@vinca.rs

presence of hysteresis phenomena (generally related to the activation temperature for a nucleation site significantly higher than the expected or theoretical value).

Modelling boiling requires many hypotheses whose validity cannot always be assessed. This results in a large number of different models, often with corrective factors. The results predicted by these models are sometimes far from the experimental results. Experiments in boiling also receive their share of difficulties. Phenomena are fast, bubbles interact, scales are multiple, material properties are not always well defined, especially the wall roughness, and physical parameters are hard to measure in fluids. Boiling needs to be simplified in order to identify the role of the different mechanisms involved. Many of the early models [4, 5] were based on bubble agitation and micro-scale convection, which are supposed to be the driving mechanism of heat transfer. These models did not include phase change, but relied on an analogy with forced convection, *i. e.*, the role of the bubble was to change the length and velocity scales used to correlate data, [6-9]. For example, the vapour-liquid exchange model on the surface of the heated wall, which was proposed by Forster and Greif [7], assumed that bubbles act as micropumps that remove a quantity of hot liquid from the wall equal to a hemisphere at the maximum bubble radius, replacing it with cold liquid from the bulk. The heat transferred from a single site was the energy required to heat this volume of liquid from the bulk temperature to the average of the wall and bulk temperatures. Theoretical models have been developed for nucleate boiling, based on a thin film evaporation concept. In these models the heat transfer from the heated wall to the rising bubble is attributed mainly to the evaporation of a thin liquid film in an area where the liquid-vapour interface approaches the wall. Some of these models are reported in [10-12].

In the present work heat transfer on heated surface in nucleate pool boiling is investigated by the application of the two-fluid model for the prediction of water-steam two-phase mixture conditions on the heated horizontal wall. The micro conditions of bubble generation at the heated wall surface are modelled by the bubble nucleation site density, the liquid wetting contact angle and the bubble growth time. The main objectives of the present work is to validate the capability of the developed numerical approach to simulate nucleate pool boiling through comparisons of simulated and experimental data from literature. For this purpose, the numerical simulations in the present work were performed for experimental conditions carried out by Theofanous [13] and Nishikawa [14].

The present paper is an extension of the previous research presented in [15, 16]. These papers are related to the numerical prediction of the Critical Heat Flux (CHF) [15] and the comparison of the boiling curve for high heat fluxes close to the CHF [16]. In [15, 16] the heat transfer form the heated wall to the boiling two-phase mixture is predicted only at the locations of bubble nucleation, while the convective heat transfer in areas between bubble nucleation sites is neglected. The model applied in the present paper takes into account the convective heat transfer from the heated wall to the boiling two-phase mixture. Namely, the conjugate heat transfer is modelled by calculation of both the heat conduction in the heated wall and the heat convection from the wetted heated wall surface to the liquid phase. The developed model is applied to the prediction of the boiling curve in the wide heat flux range, from values far from CHF values to conditions close to CHF. Therefore, regarding the previous papers [15, 16], the present paper shows an improved model that is able to predict the boiling curve in the whole range of heat flux values. In addition, the improved model is applied to the simulation of new boiling conditions that depends both on the convective heat transfer in areas between bubble nucleation sites and the heat transfer at the locations of bubble growth.

Modelling approach

Macro-scale parameters of pool boiling

Pool boiling is simulated in a square vessel, initially filled with the saturated stagnant water up to 0.02 m, fig. 1. The vessel is open to the atmosphere. The applied water level and the pressure have the same values as in the BETA physical experiments presented in [13]. The bottom wall heating starts at 0.1s after the initial time, and the calculation during this period is performed in order to establish a proper pressure field within the vessel. Vapour bubbles are generated on the heated wall at the water pool bottom, fig. 1. Upper surface of the heated wall is divided into four by four zones, fig. 1, and there is only one location within each zone that is active for the bubble rise. These locations are randomly prescribed for each zone. At the initial state, the collapsed and swell levels coincide, while later on, during the vapour generation, the swell level dynamically moves, and its position is numerically simulated. It was found that the inclusion of swell level, as the upper boundary for the liquid flow domain, is necessary in order to reliably predict the water recirculation in the pool boiling. The volume above the swell level, up to the vessel exit is filled with vapour, fig. 1. There is no water feeding during the boiling, which leads to the constant water depletion due to the evaporation. For the evaporation of the total water mass within the vessel under the high heat flux of 1500 kW/m^2, a period of approximately 27 secons is needed.

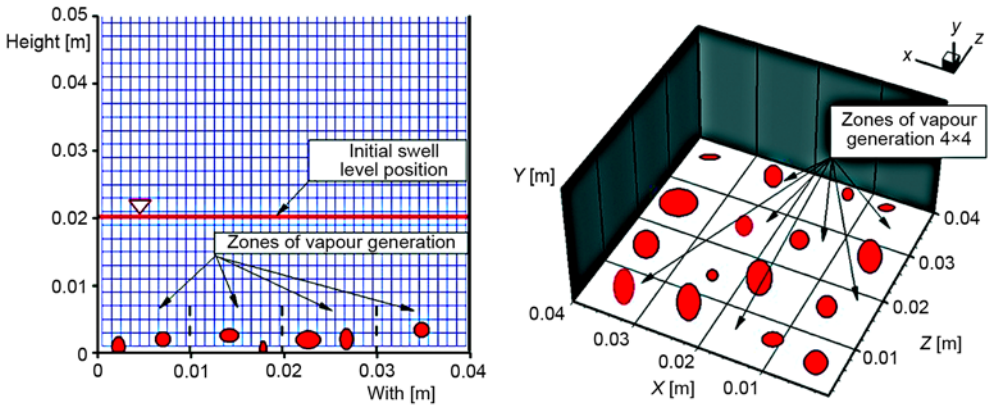

Figure 1. Water pool (left) and zones of vapour generation (right)

The quasi steady-state boiling conditions are reached after about 3 seconds of the simulation time and they are characterized with the constant amplitudes and time periods of the average wall temperature change. During this period of about 3 seconds the water mass depletion is minor compared to the total water mass in the pool and it is assumed that the water depletion has no influence on here presented computational results.

Micro-scale parameters of pool boiling

The density of nucleation sites and corresponding width of the zone for random bubble generation are input parameters for here presented simulations. Generally, the nucleation site density is determined with the heat flux, the heating surface roughness, the wetting contact angle and thermo-physical characteristics of the boiling fluid and the heated wall. The

relation between the density of nucleation sites n and the zone width b can be derived from the simple geometric condition that one square meter is covered with n nucleation sites, *i. e.*:

$$b = \frac{1}{\sqrt{n}} \tag{1}$$

Since the water pool consist of 4 × 4 zones of vapour generation, the width of the water pool equals 4*b*. This applied square dimension of the water pool is several times greater than the capillarity length defined [17]:

$$L_{\mathrm{c}} = \sqrt{\frac{\sigma}{g(\rho_1 - \rho_2)}} \tag{2}$$

The capillary length at atmospheric conditions for water equals $2.5 \cdot 10^{-3}$ m, and this value is several times smaller than the smallest width of the water pool applied in numerical simulations (for the bubble nucleation site density of 35 sites per cm^2 the applied width of the water pool is $4b = 4/(35 \cdot 10^{-4})^{-0.5} = 6.8 \cdot 10^{-3}$ m). Such geometry provides the infinity condition for the numerical simulations of vapour generation, as discussed in [13] for geometry of experimental test section.

The second parameter that determines the pool boiling dynamics is the bubble residence time on the heating surface. This is the time of bubble growth up to the bubble departure diameter. It can be predicted from the relation between bubble diameter and bubble growth time [18]:

$$D_{\mathrm{b}} = 2\left(\gamma\,\mathrm{Ja} + \sqrt{\gamma^2\,\mathrm{Ja}^2 + 2\beta\,\mathrm{Ja}}\right)\sqrt{a\tau} \tag{3}$$

where Ja is the Jacob number:

$$\mathrm{Ja} = \frac{c_p \Delta T}{h_{12}} \frac{\rho_1}{\rho_2} \tag{4}$$

The bubble diameter at the moment of separation from the wall is predicted with [19]:

$$D_{\mathrm{b}} = 0.0208\,\theta\,L_{\mathrm{c}} \tag{5}$$

where the contact angle θ is measured in degrees. No dependence of bubble departure diameter on heat flux is shown by eq. (5), but the departure diameter linearly depends on the contact wetting angle θ. The weak relation between the heat flux and the diameter of bubble at detachment is also confirmed in [20].

By substituting eq. (5) into eq. (3), the bubble residence time on the heating surface is derived in the following form:

$$\tau = \frac{(0.0208\,\theta)^2 L_{\mathrm{c}}^2}{4a\left(\gamma\,\mathrm{Ja} + \sqrt{\gamma^2\mathrm{Ja}^2 + \mathrm{Ja}^2 + 2\beta\,\mathrm{Ja}}\right)} \tag{6}$$

as the function of wetting contact angle θ and the Jacob number.

Governing equations

The 3-D liquid and vapour two-phase flow is modelled by the two fluid model [21]. Mass, momentum and energy fluid flow conservation equations are written for both liquid and

vapour phase, while interface transfer processes are modelled by *closure laws*. This approach implies non-equilibrium thermal and flow conditions.

The two-phase flow is observed as semi-compressible, that is the acoustic flow effects are neglected, while the influence of the pressure and temperature change on the vapour and liquid thermo-physical properties is taken into account. The surface tension is neglected, as it is not important for bulk two-phase flow phenomena. Hence, pressure is the same for both phases within the numerical control volume. Conservation equations take the following form in the index notation:

– Mass conservation equation:

$$\frac{\partial \alpha_k \rho_k}{\partial t} + \frac{\partial (\alpha_k \rho_k u_{k,i})}{\partial x_i} = (-1)^k (\Gamma_e - \Gamma_c) \tag{7}$$

– Momentum conservation equation:

$$\frac{\partial (\alpha_k \rho_k u_{k,i})}{\partial t} + \frac{\partial (\alpha_k \rho_k u_{k,i} u_{k,j})}{\partial x_i} = -\alpha_k \frac{\partial p}{\partial x_i} + \frac{\partial}{\partial x_j}\left(\alpha_k \rho_k \nu_k \frac{\partial u_{k,i}}{\partial x_j} \right) \alpha_k \rho_k g_i +$$

$$+(-1)^k (\Gamma_e - \Gamma_c) \partial u_{k,i} + (-1)^{k+1} F_{2l,i} \tag{8}$$

– Energy conservation equation:

$$\frac{\partial (\alpha_k \rho_k T_k)}{\partial t} + \frac{\partial (\alpha_k \rho_k u_{k,i} T_k)}{\partial x_i} = \frac{\partial}{\partial x_j}\left(\frac{k_k}{c_{p,k}} \frac{\partial T_k}{\partial x_i} \right) \alpha_k \rho_k g_i + (-1)^k (\Gamma_e - \Gamma_c) T_k + \frac{(2-k)\dot{q}_b}{c_{p,k}} \tag{9}$$

where index values $k = 1$ and $k = 2$ denote liquid and vapour respectively. The source terms of mass, momentum and thermal energy interface transfer are written on the right hand side of eqs. (7)-(9). The rate of phase transition, which is the mass of evaporation or condensation per unit volume and time, are denoted with Γ_e and Γ_c, respectively. The force of vapour and liquid interfacial drag per unit volume in i Cartesian direction is denoted with $F_{2l,i}$. The volume fraction balance is added to the previous system of equations:

$$\alpha_1 + \alpha_2 = 1 \tag{10}$$

Energy equation for the heated wall is:

$$\frac{\partial T}{\partial t} = a \nabla^2 T + \frac{\dot{q}_h}{(\rho c_p)_p} - \frac{\dot{q}_b}{(\rho c_p)_p} \tag{11}$$

where q_h is the volumetric heat source in the wall (applicable for instance in case of wall electrical heating), and q_b – the heat sink in control volumes on the heated wall surface due to the bubble growth. In eq. (9) parameter $\dot{q}_b$ represents the heat source in the fluid control volumes at the bottom of the pool where the bubble growth occurs. It is assumed that the bubble nucleation does not occur, *i. e.* the heat source $\dot{q}_b$ equals zero, if the void fraction in the control volume on the wall surface is higher than $1\text{-}10^{-5}$. The volumetric heat power $\dot{q}_b$ is defined as the ratio of heat necessary for the bubble growth and the bubble growth time till departure as $\dot{q}_b = \pi D_b^3 \rho_2 r / 6\tau$.

Closure Laws

The interfacial drag force per unit volume of computational cell is calculated as [21]:

$$F_{2l,i} = \frac{3}{4}\alpha_2\rho_1\frac{C_\mathrm{D}}{D_\mathrm{P}}\sqrt{\sum_{j=1}^{3}(u_{2,j}-u_{1,j})^2}\,(u_{2,j}-u_{1,j}) \tag{12}$$

where C_D is the interfacial drag coefficient, and D_P is the diameter of the dispersed particle. The correlation for the interfacial drag coefficient C_D is proposed in the form:

$$C_\mathrm{D} = 1.487 D_\mathrm{P}\left(\frac{\mathrm{g}\Delta\rho}{\sigma}\right)^{1/2}(1-\alpha_2)^3(1-0.75\alpha_2)^2 \tag{13}$$

where the dependence on the mixture void fraction α_2 has the same function form as the CATHARE code correlation [22] for the interface friction in the transitional two-phase flow patterns.

The intensity of evaporation and condensation rate is calculated with the empirical model that takes into account the relaxation time of evaporation τ_e and condensation τ_c ($\tau_\mathrm{e} = \tau_\mathrm{e} = = 0.02$ s).

$$\Gamma_\mathrm{e} = k_\mathrm{e}\alpha_1(T_1 - T_2'') = \frac{\alpha_1\rho_1}{\tau_\mathrm{e}}(T_1 - T_2'') \tag{14}$$

$$\Gamma_\mathrm{c} = k_\mathrm{c}\alpha_1(T_2'' - T_1) = \frac{\alpha_1\rho_1}{\tau_\mathrm{c}}(T_2'' - T_1) \tag{15}$$

Boundary conditions

Adiabatic boundary conditions are prescribed for the velocity components at the lateral vertical plane and the top exit plane of the water pool (*i. e.* there is no change of the velocity components in the direction perpendicular to the plane), except the velocity components perpendicular to the lateral planes, which equal zero, fig. 2. Also, the velocity is zero on the heated wall top surface. The adiabatic temperature boundary conditions are prescribed on the lateral vertical planes and on the top exit plane of the water pool. The uniform heat flux q_A is prescribed at the bottom surface of the heated wall, while the lateral sides of the heated wall are adiabatically insulated. The random bubble generation is prescribed for each of 4 by 4 zones at the top of the heated wall by number random function available in the computer code compiler. These randomly chosen control volumes at the top of the heated wall are heat sinks, while adjacent control volumes in the pool are heat sources for liquid evaporation. In the area of heated wall without the bubble generation, the conjugate convection from the wall to the liquid phase is assumed. In the previous work on numerical modelling of the critical heat flux [15, 16], it was assumed that the major portion of the heat is transferred at the nucleation sites, fig. 2, and the heat transfer by convection from the heated wall to the liquid was neglected. In the present research, the convective heat transfer is taken into account. These boundary conditions are presented in tabs. 1 and 2.

Numerical method

The control volume based finite difference method is applied for the numerical solution of the set of balance eq. (7)-(9) and (11). A pressure-correction equation is derived according to the SIMPLE numerical method [23] from the momentum and mass balance equations. The 3-D flow field is discretized in Cartesian co-ordinates. Numerical grid consists of two parts: the heated wall (40×10×40 control volumes) and the water pool (40 × 70 × 40 control volumes). The grid refinement test was performed with the grid 80 × 20 × 80 for the wall and 80 × 140 × 80 for the water pool.

Table 1. Boundary conditions for the water pool

At the left vertical plane	$x = 0,\quad 0 \le y \le H,\quad 0 \le z \le a,\quad u = 0,\quad \frac{\partial v}{\partial x} = 0,\quad \frac{\partial w}{\partial x} = 0,\quad \frac{\partial T}{\partial x} = 0$
At the right vertical plane	$x = a,\quad 0 \le y \le H,\quad 0 \le z \le a,\quad u = 0,\quad \frac{\partial v}{\partial x} = 0,\quad \frac{\partial w}{\partial x} = 0,\quad \frac{\partial T}{\partial x} = 0$
At the back vertical plane	$0 \le x \le a,\quad 0 \le y \le H,\quad z = 0,\quad \frac{\partial u}{\partial z} = 0,\quad \frac{\partial v}{\partial z} = 0,\quad w = 0,\quad \frac{\partial T}{\partial z} = 0$
At the front vertical plane	$0 \le x \le a,\quad 0 \le y \le H,\quad z = a,\quad \frac{\partial u}{\partial z} = 0,\quad \frac{\partial v}{\partial z} = 0,\quad w = 0,\quad \frac{\partial T}{\partial z} = 0$
At the bottom horizontal plane on the heated wall	$0 \le x \le a,\quad y = 0,\quad 0 \le z \le a,\quad y = v = w = 0,\quad \left(\lambda \frac{\partial T}{\partial y}\right)_{\mathrm{w}} = \left(\lambda \frac{\partial T}{\partial y}\right)_{1}$
At the top horizontal plane	$0 \le x \le a,\quad y = H,\quad 0 \le z \le a,\quad \frac{\partial u}{\partial y} = 0,\quad \frac{\partial v}{\partial y} = 0,\quad \frac{\partial w}{\partial y} = 0,\quad \frac{\partial T}{\partial y} = 0$

Table 2. Boundary conditions for the heated wall

Lateral walls	$\frac{\partial T}{\partial x} = 0,\quad \frac{\partial T}{\partial z} = 0,\quad 0 < x < a,\quad 0 < z < a,\quad 0 \le y \le \delta$
Top wall	$\left(\lambda \frac{\partial T}{\partial y}\right)_{\mathrm{w}} = \left(\lambda \frac{\partial T}{\partial y}\right)_{1},\quad 0 \le x \le a,\quad y = \delta,\quad 0 \le z \le a$
Bottom wall	$q_A = \text{const.} = \lambda \frac{\partial T}{\partial y}$

A discretization of partial differential equations is carried out by their integration over control volumes of basic and staggered grids. The convection terms are approximated with upwind finite differences, while diffusion and source terms are approximated with central differences. Fully implicit time integration is applied. The resulting set of algebraic equations is solved iteratively with the line-by-line three-diagonal-matrix algorithm (TDMA). The calculation error for every balance equation and every control volume is kept within prescribed limits by iterative solution of sets of linear algebraic equations. The criterion for the overall calculation procedure solution is the fulfilment of the mass balance for every control volume within prescribed relative error of 10^{-6}. Also, this criterion implies that the overall mass balance, for the whole flow field is achieved.

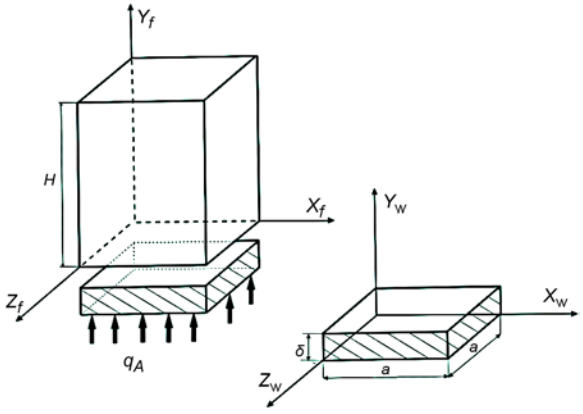

Figure 2. Clation domains for the water pool (upper volume) and healcuated wall (lower volume)

Results

Figure 3 shows 3-D view at the void fraction distribution in pool boiling for four different values of the heat flux 200 kW/m^2, 500 kW/m^2, 700 kW/m^2, and 1400 kW/m^2. Vapour bubbles form at discrete sites on the heated surface. The frequency of bubble release and the number density of active nucleation sites increase with the heat flux. In case of heat flux value of 200 kW/m^2, (top-left figure), swell level is almost plane and its value is about 0.03 m. Large number of departed bubbles can be observed. In case of higher heat flux value of 500 kW/m^2, (top right figure 3), the swell level position is higher and typical bursting of large vapour lumps is observed at the swell level. Also, the formation of vapour layers at certain parts of the bottom heating wall is observed. Figure 3 at the bottom left and right for heat flux values of q = 700 kW/m^2, and q = 1400 kW/m^2, shows large vapour columns through the whole volume of vessel, which are formed due to intensive vapour generation, as well as due to the merging of several vapour lumps into the larger one. In case of the heat flux value of 1400 kW/m^2, almost the whole volume is filled with vapour.

Figure 4 (left) shows vapour blankets formation on the heater's surface for heat flux value of q = 500 kW/m^2. It is clearly seen that the vapour spots are formed at the nucleation sites, which locations are randomly chosen within hundred (10×10) cells of the 4×4 zones at the heater

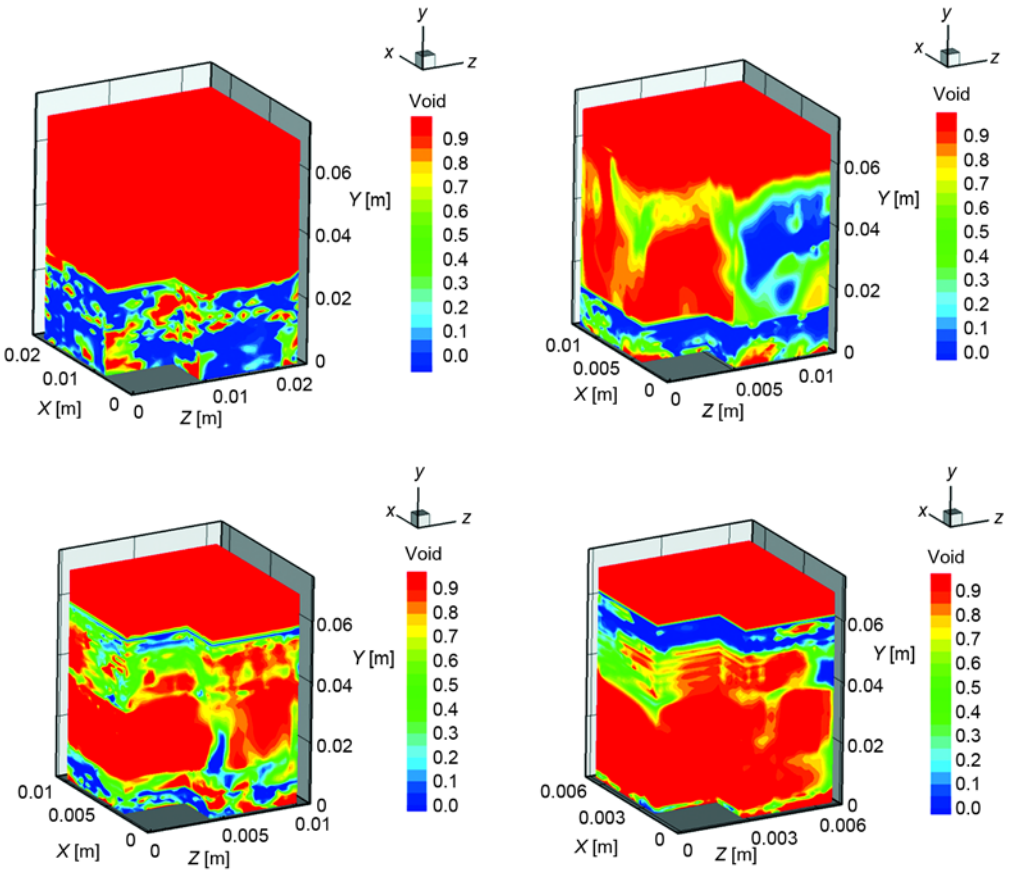

Figure 3. The 3-D view of void fractions at the pool boiling (heat flux q = 200 kW/m^2 – top-left, q = 500 kW/m^2 – top-right; q = 700 kW/m^2 – left; q = 1400 kW/m^2 – right) *(for color image see journal web-site)*

surface. Figure 4 (right) shows temperature field at the top surface of the heated wall. The temperatures at the locations of bubbles' nucleation are significantly lower, thereby showing the effectiveness of heat transfer by evaporation. These are spots of heat sink at the top surface of the heated wall, because the heat is conducted to the locations of bubbles' growth. It can be observed that the temperature is much higher in the areas around the locations of the bubbles nucleation, where the heat is transferred from the wall to the liquid only by conjugate conduction. The steam in the two-phase mixture on the heated wall is saturated, while the water is superheated over the saturation temperature only in the first layer of control volumes on the wall surface.

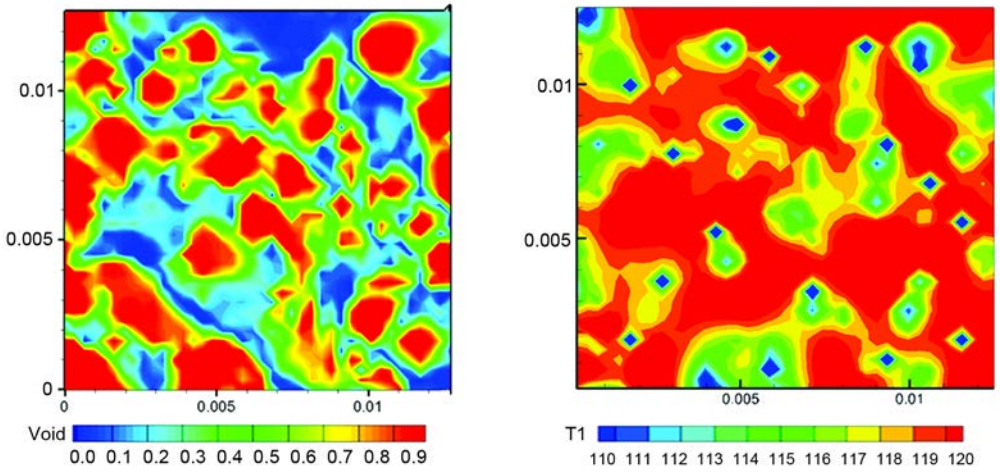

Figure 4. The 2-D planes of void fractions at nucleation sites at the heated wall-left; temperature distribution on the heated surface-right *(for color image see journal web-site)*

The diagram in fig. 5 shows that the averaged void value at the heater's surface is approximately 0.5, then it drops to the value of nearly 0.1 within the pool boiling mixture and rises above the height of 0.02 m. The heat flux dependence on nucleation site density is presented in fig. 6. The results are compared with the experimental data obtained by Theofanus

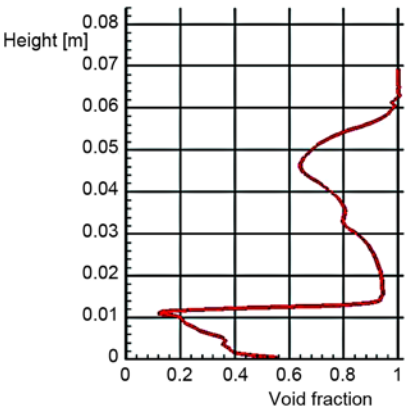

Figure 5. Averaged void fraction in the pool (q = 500 kW/m^2)

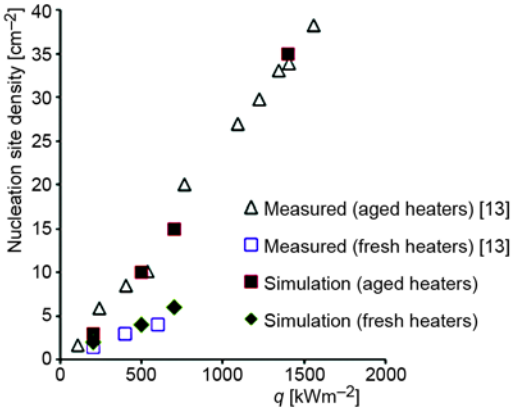

Figure 6. Nucleation site density as a function of the heater's heat flux

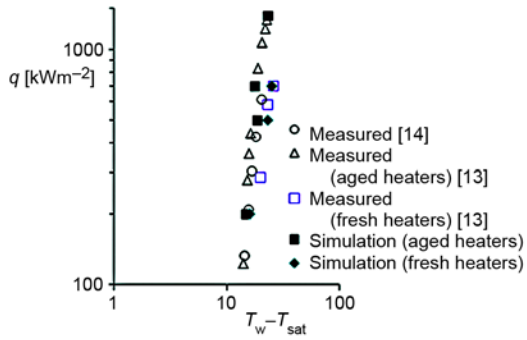

Figure 7. Effect of wall superheat on heat transfer

[13] for nucleate boiling on aged and fresh heaters. The good agreement is obtained between calculated and measured data. The dependence is linear and the nucleation site density increases with the heat flux increase. Figure 7 shows the variation of heat flux with wall superheat over the saturation temperature. In the numerical simulation the heat flux at the bottom of the heated wall is prescribed, while the average temperature of the top wall surface in contact with the two-phase mixture T_w is calculated as the mean value of the wall temperatures in all control volumes in the layer at the top of the wall, these results are obtained by the solving of the heat conduction eq. (11). Numerical results are compared with the experimental data obtained by Theofanous [13] and Nishikawa [14], and they show very good agreement. As already stated, the bubble nucleation site density is the input parameter in here presented numerical simulations and it depends on the heated wall roughness and aging, as well as boiling liquid wetting ability and present impurities, as it was analysed in [13]. Comparison of the results obtained both experimentally and numerically for the aged and fresh heaters in figs. 6 and 7 shows that the fresh heaters have lower nucleation site densities and they lead to the higher wall superheat for the same heat flux.

Grid refinement test was performed with the numerical mesh with doubled number of control volumes (80 × 140 × 80 grid) in comparison to the grid with 40 × 70 × 40 control volumes, which is applied in the above presented simulations. It was shown that the difference between mean temperatures of the heated wall top surface in simulations with fine and coarser grid is less than 0.5 K. In addition, there were no practical differences in pool two-phase mixture behaviour and wall temperature field for these two cases.

Conclusions

This work represents a comprehensive CFD analysis of nucleate pool boiling in a square vessel of saturated water under atmospheric conditions. This analysis also served as a method to validate the capabilities of the new numerical model to simulate nucleate pool boiling, by comparisons with experimental data available in the literature. Four cases of simulations were carried out and the simulation results are compared with experimental data and their good agreement is found.

The developed modelling and numerical methodology revealed that the combined application of the basic deterministic conservation laws for the continuous two-phase flow field and the stochastic characteristics of the vapour generation at the heated wall are able to simulate complex pool boiling conditions. Obtained results on two-phase mixture structure in pool boiling and temperature field at the heater surface, show that the applied algorithm for the prediction of heating wall boundary conditions takes into account the complex micro scale effects. Stable and efficient calculations for different values of nucleation site density and bubble residence time demonstrate the robustness of the applied numerical approach. The developed numerical method could be a support to the investigation of the influence of the micro mechanisms of nucleate boiling on the heated wall temperature field and two-phase mixture behaviour in pool boiling.

Acknowledgment

This work has been supported by the Ministry of Education, Science and Technological Development of the Republic of Serbia (grants TR-33018 and OI-174014).

Nomenclature

a – thermal diffusivity, [m^2s^{-1}]
b – width of the nucleation zone, [m]
C_D – interfacial drag coefficient [–]
c_p – specific heat, [$Jkg^{-1}K^{-1}$]
D – diameter, [m]
D_b – bubble departure diameter, [m]
F – force per unit volume, [Nm^{-3}]
g – gravitational acceleration, [ms^{-2}]
Ja – Jacobs number, [–]
k – thermal conductivity, [$Wm^{-1}K^{-1}$]
L_c – water capillary length, [m]
n – density of nucleation sites, [m^{-2}]
p – pressure, [Pa]
q – heat flux, [Wm^{-2}]
q_b – volumetric heat source for bubble generation on the heater's surface, [Wm^{-3}]
q_h – volumetric heat rate, [Wm^{-3}]
T – temperature, [K]
t – time, [s]
u – velocity, [ms^{-1}]
x – co-ordinate,[m]

Greek symbols

α – void fraction, [–]
β – empirical constant, [–]
Γ – phase transition rate, [$kgm^{-3}s^{-1}$]
γ – empirical constant, [–]
θ – wetting contact angle, [°]
ρ – density, [kgm^{-3}]
ν – kinematic viscosity, [m^2s^{-1}]
σ – surface tension, [Nm^{-1}]
τ – phase change relaxation time, [s]

Subscripts

b – bubble
c – condensation
e – evaporation
k – phase index (k = 1, 2)
p – particle
sat – saturation
w – wall
1 – water
2 – steam
21 – interfacial
“ – saturated vapour

References

[1] Zhang, B. J., Kim, K. J., Nucleate Pool Boiling Heat Transfer Augmentation on Hydrophobic Self-Assembly Mono-Layered Aluminia Nano-Porous Surfaces, *Int. J. Heat Mass Transfer,* 73 (2014), June, pp. 551-561
[2] Xu, P., *et al.*, Enhanced Boiling Heat Transfer on Composite Porous Surface, *Int. J. Heat Mass Transfer, 80* (2015), Jan., pp. 107-114
[3] Sanna, A., *et al.*, Numerical Investigation of Nucleate Boiling Heat Transfer on Thin Substrates, *Int. J. Heat Mass Transfer, 76* (2014), Sep., pp. 45-64
[4] Stojanovic, A., *et al.*, Review of Heat Transfer Mechanisms in Pool Boiling, *Proceedings*, Int. Conf. Power Plants, Zlatibor, Serbia, 2014, pp. 729-743
[5] Kim, J., Review of Nucleate Pool Boiling Bubble Heat Transfer Mechanisms, *Int. J. Multiphase Flow, 35* (2009), 12, pp. 1067-1076
[6] Rohsenow, W. M., A Method of Correlating Heat Transfer Data for Surface Boiling of Liquids, *Trans. ASME 4* (1952), 7, pp. 969-975
[7] Forster, H. K., Greif, R., Heat Transfer to a Boiling Liquid – Mechanisms and Correlations, *J. Heat Transfer 81* (1959), 2, pp. 45
[8] Zuber, N., Nucleate Boiling the Region of Isolated Bubbles and the Similarity with Natural Convection, *Int. J. Heat Mass Transfer, 6* (1963), 7, pp. 53-78
[9] Tien, C. L., A Hydrodynamic Model for Nucleate Pool Boiling, *Int. J. Heat Mass Transfer, 5* (1962), 3, pp. 533-540
[10] Stephan, P., Kern, J., Evaluation of Heat and Mass Transfer Phenomena in Nucleate Boiling, *Int. J. Heat Fluid Flow, 25* (2004), 2, pp. 140-148
[11] Wayner, P. C., *et al.*, The Interline Heat Transfer Coefficient on an Evaporating Wetting Film, *Int. J. Heat Mass Transfer 19*, (1976), 5, pp. 487-492

[12] Mitrovic, J., The Flow and Heat Transfer in the Wedge-Shaped Liquid Film Formed during the Growth of a Vapour Bubble, *Int. J. Heat Mass Transfer, 41* (1998), 12, pp. 1771-1785
[13] Theofanous, T. G., *et al.*, The Boiling Crises Phenomenon, *Experimental Thermal and Fluid Science, 26* (2002), 6-7, pp. 775-792
[14] Nishikawa, K., *et al.*, Effect of Surface Configuration on Nucleate Boiling Heat Transfer, *Int. J. Heat Mass Transfer, 27* (1984), 9, pp. 1559-1571
[15] Pezo, M., Stevanovic, V., Numerical Prediction of Critical Heat Flux in Pool Boiling with the Two-Fluid Model, *Int. J. Heat Mass Transfer, 54* (2011), 15-16, pp. 3296-3303
[16] Pezo, M., Stevanovic, V., Numerical Prediction of Nucleate Boiling Heat Transfer Coefficient under High Heat Fluxes, *Thermal Science 20* (2016), Suppl. 1, pp. S113-S123
[17] Jacob, M., Linke, W., Heat Transfer by Liquid Evaporation on Vertical and Horizontal Surfaces (in German), *Phys. Z, 8* (1935), 6, pp. 267-280
[18] Isachenko, V. P., *et al*., *Heat Transfer,* Mir Publisher, Moscow, 1980
[19] Fritz, W., Calculation of Maximal Bubble Volume (in German), *Physikalische Zeitschrift, 36* (1935), 8, pp. 379-384
[20] Sakashita, H., Kumada, T., Method for Predicting Curves of Saturated Nucleate Boiling, *Int J. Heat Mass Transfer, 44* (2001), 3, pp. 673-682
[21] Ishii, M., Two-Fluid Model for Two-Phase Flow, 2nd Int. Workshop on Two-Phase Flow Fundamentals, Rensselaer Polytechnic Institute, Troy, N. Y., USA, 1987
[22] Rousseau, J. C., Houdayer, G., Advanced Safety Code CATHARE Summary of Verification Studies on Separate Effects Experiments, *Proceedings*, 2nd International Topical Meeting on Nuclear Reactor Thermal-Hydraulics 2, Santa Barbara, Cal., USA, 1983
[23] Patankar, S., *Numerical Heat Transfer and Fluid Flow*, Hemisphere Publ. Co., New York, USA, 1980

Paper submitted: April 4, 2016
Paper revised: July 1, 2016
Paper accepted: July 3, 2016